Chapter 4

Antisite disorder induced Berry phase and anomalous Hall conductivity in Co_2FeAl Heusler compound

This work is authored by Gaurav K. Shukla et al. and published in Phys. Rev. B 105, 035124 (2022).

This chapter involves the study of the effect of the antisite disorder on the anomalous Hall effect (AHE) in Co_2FeAl Heusler compound. Co_2FeAl Heusler compound crystallizes in the B2 type structure, which provides an avenue to investigate the disorder effect on the AHE. The combined experimental and theoretical results establish that the antisite disorder can enhance the AHC of the system, which is in contrast to the prior studies suggesting that the disorder decreases the anomalous Hall conductivity (AHC) in the system.

4.1 Introduction

In this chapter, we studied the anomalous Hall effect (AHE) in the Co_2FeAl Heusler compound. Co-based full Heusler compounds got enormous attention for their half-metallic behavior, high Curie temperature, and 100% spin-polarization around the Fermi level, which are the most prominent properties useful in spintronics devices and other memory-based applications [1–4]. Additionally, Co-based Heusler compounds are of current interest, because of their large AHE due to the large Berry curvature linked with their band structure [5–9]. The intrinsic AHE arises due to the Berry curvature associated with the Bloch bands. It is noteworthy here that the Berry curvature is highly sensitive to the electronic band structure of material and modulation in the band structure can influence the Berry curvature and hence intrinsic anomalous Hall conductivity (AHC) [10]. The disorder may change the topology of the Fermi-surface or position of the Fermi level or modify the local potential environment that breaks the translational symmetry, inevitably modifying the band structure, which may reshape the AHE [9–13]. An increased anomalous transport response has been reported in the thin film of $Co_2MnAl_{1-x}Si_x$ due to increased $L2_1$ ordering within the lattice [12]. Recently, the enhancement in the AHC has been observed in Fe_2-based high Curie temperature Heusler compounds due to the increase in the crystal symmetry, when the system transforms from inverse Heusler to B2 type (CsCl) structure [14].

Among Co-based Heusler compounds, Co_2FeAl is the most prominent candidate for data processing and storage-based applications due to its large Curie temperature($\sim$ 810 K to 900 K), high spin-polarization, low gilbert damping factor, and ultrafast magnetization dynamics [15–19]. As the literature suggests that the Co_2FeAl is generally crystallized in B2-type [17, 20–22] disordered structure, therefore, this compound provides an opportunity for the investigation of the disorder

effect on the Berry curvature and intrinsic AHC. Attempts to investigate anomalous transport in Co_2FeAl thin films report controversial results concerning the origin of AHE [20, 21, 23].

In this work, we studied AHE in a polycrystalline bulk Co_2FeAl Heusler compound. Synchrotron x-ray diffraction (SXRD) data reveals a large degree of antisite disorder between Fe and Al atoms. The experimental value of AHC was found to be about 227 S/cm at 2 K and 219 S/cm at 300 K with an intrinsic contribution of 155 S/cm. This intrinsic value of AHC is an order of magnitude larger than the theoretically predicted AHC for an ordered $L2_1$ phase of Co_2FeAl. Our theoretical calculations show that the antisite disorder in Co_2FeAl enhances the Berry curvature-induced intrinsic AHC.

4.2 Methods

A polycrystalline Co_2FeAl Heusler compound was synthesized using a conventional arc melting technique using a stoichiometric amount of its highly pure constituent elements. The compound was melted four times to ensure chemical homogeneity. A very small weight loss of 0.32% was noted after melting. Further, the ingot was sealed in a quartz ampoule under Ar atmosphere and then annealed at 800°C for 12 hours for better homogeneity. A small piece was cut from the annealed ingot and crushed into powder for SXRD measurement. The SXRD measurement was performed at PETRA-III, DESY for structural analysis using a wavelength of 0.207 Å. Magnetic field-dependent magnetization measurements were carried out using the Magnetic Property Measurement System (MPMS) from Quantum Design, U.S.A. A small polished rectangular piece was used for four-probe and five-probe magneto-transport measurements to obtain the longitudinal resistivity (ρ_{xx}) and the Hall resistivity (ρ_H), respectively. To obtain the actual ρ_H, raw Hall resistivity data ($\rho_H{}^{raw}$) was anti-symmetrized by averaging the difference of $\rho_H{}^{raw}$ at the positive and negative magnetic fields.

Electronic structure calculations were carried out using pseudo-potential based density-functional theory and plane-wave basis sets as implemented in Quantum ESPRESSO (QE) [24], whereas the exchange-correlation potential is approximated through PBE-GGA functional [25]. Optimized norm-conserving Vanderbilt pseudo-potentials [26] are used in the calculations and the kinetic energy cutoff for the plane wave is taken as 80 Ry. The electronic integration over the Brillouin zone is approximated by the Gaussian smearing of 0.01 Ry both for the self-consistent (SC) and non-self-

consistent (NSC) calculations. The threshold for the SC energy calculations is taken as $10^{-8} Ry$. The projections of Bloch wave functions are made into maximally localized Wannier functions. Wannier90 tool (implemented within QE) has been used to compute the Wannier interpolated bands and AHC [24, 27, 28]. SOC is introduced in all the calculations. The Monkhorst-Pack $\boldsymbol{k}$-grid of $8 \times 8 \times 8$ are considered in the SC, NSC and Wannier90 calculations. The transition metal-d and Al-p orbitals are used as the projections for the Wannier90 calculations. The AHC calculation is carried out with a dense $\boldsymbol{k}$-grid of $75 \times 75 \times 75$. Further, through the adaptive refinement technique, a fine mesh of $5 \times 5 \times 5$ is added around the points wherever the mode of the Berry curvature ($|\Omega(\boldsymbol{k})|$) exceeds 100 bohr^2. The calculations are carried out using experimental lattice parameter.

4.3 Result and discussion

4.3.1 Structural analysis

The SXRD pattern of Co_2FeAl compound was collected at room temperature for a detailed structural study. In the first step, the Rietveld refinement of the SXRD pattern was carried out using the $L2_1$ ordered cubic structure with space group $Fm\bar{3}m$. For the refinement, all the atoms were considered at special positions i.e. Co at 8c (0.25,0.25,0.25), Fe at 4b (0.5, 0.5, 0.5), and Al at 4a (0, 0, 0) Wyckoff positions, respectively. The result of refinements is shown in Fig. 4.1(a). We noticed the presence of (111) superlattice reflection in the calculated x-ray diffraction (XRD) pattern (black lines of Fig. 4.1(a)), while this reflection is completely absent in the observed XRD pattern (red dots in Fig. 4.1(a)), which indicates the presence of antisite disorder in the Co_2FeAl compound. Recently the mixed $L2_1$ and B2 phase was observed in Co_2FeAl ultrathin film [29]. We would like to mention here that an attempt to anneal the Co_2FeAl at different temperatures could not show a different XRD pattern as compared to the one observed in Fig. 4.1(a). It is important to remark here that atomic disorder is a common phenomenon in Heusler compounds [11, 12, 30]. The available literature also suggests that the most stable structure of Co_2FeAl is the B2 type structure i.e. there is antisite disorder between Fe and Al atoms [17, 20–22]. So, in the next step, we simulated the XRD pattern of Co_2FeAl considering Fe-Al antisite disorder in such a way that the total number of Fe and Al atoms remains the same. For the XRD simulation, we used PowderCell software [31]. It

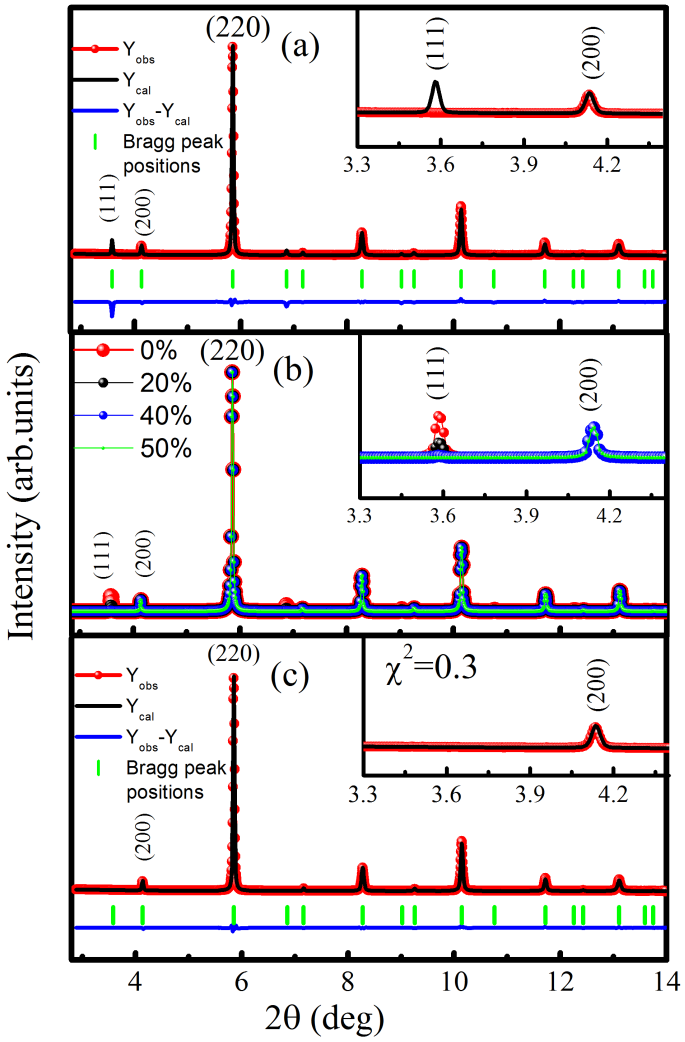

Figure 4.1: (a) Rietveld refinement of room temperature (RT) synchrotron x-ray diffraction (SXRD) pattern of Co_2FeAl considering ordered $L2_1$ structure. (b) Simulated XRD patterns considering Fe and Al antisite disorder with indicated percentage. (c) Rietveld refinement of RT SXRD pattern of Co_2FeAl with 50% Fe and Al antisite disorder. Insets of figures show an enlarged view around (111) and (200) superlattice reflections.

is clear from Fig.4.1(b), that the intensity of (111) peak decreases with an increase in the amount of disorder and vanishes completely at about 50% antisite disorder between Fe-Al atoms. Therefore, finally, we performed the Rietveld refinement of the SXRD data assuming 50% antisite disorder between Fe-Al atoms, which could fit the Bragg peaks very well [Fig.4.1(c)] and confirms the phase purity (cubic) as well as large antisite disorder (B2 type) in the sample. Moreover, the presence of (200) Bragg peak primarily indicates the formation of ordered Co-sublattice and also precludes the possibility of A2 disorder (atomic disorder among all sites) in the sample. The intensity ratio of superlattice reflection (200) and the fundamental reflection (220) (i.e. $\frac{I_{200}}{I_{220}}$) was found to be 0.048

and 0.046 from the experimental SXRD pattern and simulated XRD pattern, respectively are nearly same and further confirms the ordered Co-sublattice in the present compound [20]. The refined unit cell parameter was found to be 5.73 Å, which is in good agreement with the literature [32, 33].

4.3.2 Magnetization and resistivity

The magnetic moment obtained from the magnetic isotherms (Fig.4.2) is about 5.74 μ_B/f.u and 5.50 μ_B/f.u at 2 K and 300 K, respectively, which is close to the value reported in the literature [17, 22, 33–37]. The variation of ρ_{xx} as a function of temperature (Fig.4.3(a)) depicts that ρ_{xx} increases with increasing temperature, indicating the metallic character of the compound. The residual resistance ratio (RRR = $\frac{\rho_{xx}(300\,K)}{\rho_{xx}(2\,K)}$) about 1.25 is similar to the reported value for other Co-based Heusler compounds [5, 38, 39].

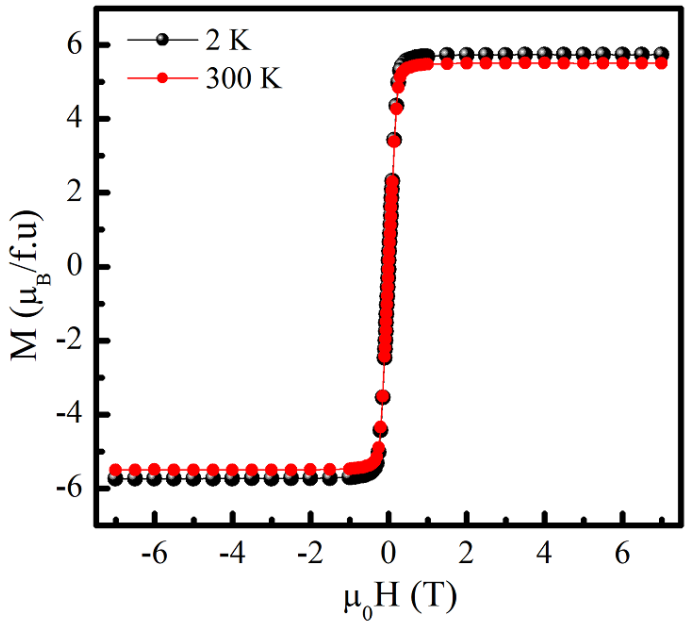

Figure 4.2: Magnetic isotherms ($M - H$ curves) recorded at 2 K and 300 K.

4.3.3 Anomalous Hall

We carried out detailed magneto-transport measurements in a wide temperature range of 2 K-300 K to study the AHE in the Co_2FeAl. The Hall resitivity (ρ_H) can be given by the equation, $\rho_H = R_0 H + R_s M$, where R_0, R_s are the normal and anomalous Hall coefficients, respectively. ρ_H versus H were measured at different temperatures up to a field of 7 Tesla (T). From Fig.4.3(b), it is evident

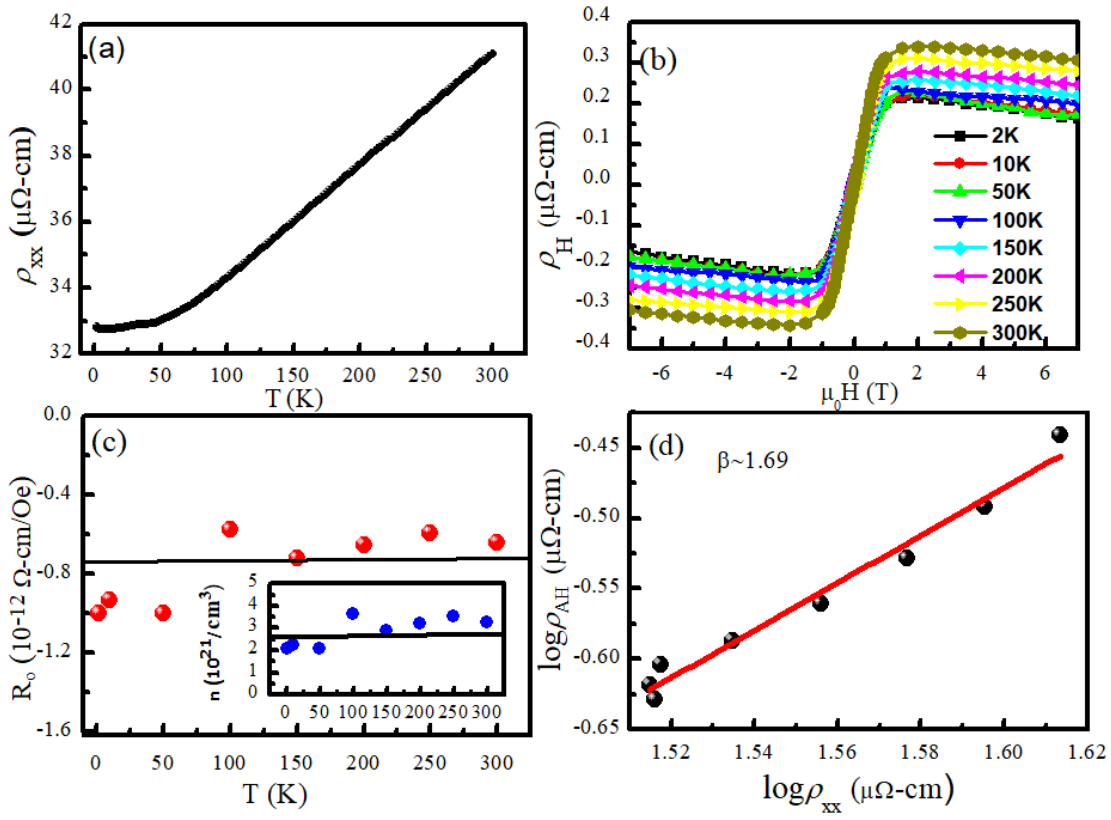

Figure 4.3: (a) Temperature dependent longitudinal resistivity ρ_{xx}. (b) Field dependent Hall resistivity ρ_H at different temperatures. (c) Temperature-dependent normal Hall coefficient R_0. The inset shows temperature variation of carrier concentration n. (d) Experimental data (black dots) plotted between logρ_{AH} and logρ_{xx} and the fitted curve is shown in red color.

that ρ_H steeply increases with field up to 1 T, which can be observed due to AHE. However, under the application of higher fields ($>$1 T), a negative slope is noted due to the ordinary Hall effect. The normal Hall coefficient (R_0) was calculated from the slope of the high field ρ_H curve. Fig.4.3(c) shows temperature variation of R_0. The negative value of R_0 indicates the electrons are the majority charge carriers. Inset of Fig.4.3(c) shows the magnitude of carrier concentration (n) at different temperatures, calculated using the relation, R_0=$\frac{1}{ne}$ and n was found to be around 3×10^{21} at 300 K and variation of n with temperature is little scattered. The anomalous Hall resistivity (ρ_{AH}) was calculated by extrapolating the high field ρ_H curve on the y-axis at zero field.

To elucidate the mechanism giving rise to AHE, we have plotted ρ_{AH} versus ρ_{xx} on a double logarithmic scale and fitting was employed to determine the exponent β using the relation $\rho_{AH} \propto {\rho_{xx}}^{\beta}$ [5] as shown in Fig.4.3(d). If β=1, the origin of AHE is assigned to the skew scattering, and if β =2, the origin of AHE is due to intrinsic and side jump mechanisms [5]. We found the exponent $\beta = 1.69$,

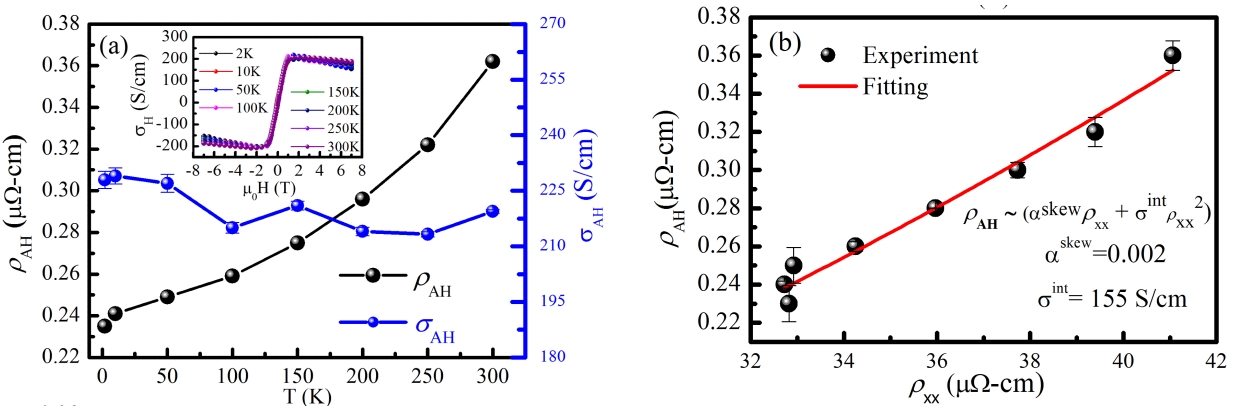

Figure 4.4: (a) Anomalous Hall resistivity ρ_{AH} and anomalous Hall conductivity σ_{AH} as a function of temperature. The inset shows field-dependent Hall conductivity isotherms. (b) Experimental data (black dots) plotted as ρ_{AH} versus ρ_{xx}. The fitted curve is shown in red color.

which indicates that the AHE in Co_2FeAl is dominated by the intrinsic and side jump mechanisms. The contribution of side jump in AHC can be estimated using an expression $(e^2/(ha))(\epsilon_{so}/E_F)$, where ϵ_{so} is the spin–orbit interaction and E_F is Fermi energy [40, 41]. The terms e, h, and a are the electronic charge, Planck constant, and lattice parameter, respectively. For most of the ferromagnetic metals, ϵ_{so}/E_F is the order of 10^{-2}, and hence the very small contribution of AHC is expected due to side jump in comparison to the intrinsic part of AHC. However, it is not possible to decouple the intrinsic and side jump mechanisms practically because both have similar dependencies on ρ_{xx}. We have calculated the Hall conductivity using tensor conversion $\sigma_H = \frac{\rho_H}{(\rho_H{}^2+\rho_{xx}{}^2)}$ [30, 42] as shown in inset of Fig. 4.4(a). The AHC is calculated by averaging of extrapolated values of the high-field Hall conductivity curve at zero fields of the positive and negative field directions. Temperature-dependent ρ_{AH} (black dots) and AHC (blue dots) are shown in Fig.4.4(a). The value of AHC is found to be about 227 S/cm at 2 K and does not show appreciable change at 300 K (219 S/cm). The variation of AHC is nearly temperature-independent, suggesting that the origin of AHE is intrinsic [43, 44]. To separate the extrinsic and intrinsic part of AHE, we have plotted ρ_{AH} versus ρ_{xx} and fitted [Fig.4.4(b)] according to well establish an equation for AHE, $\rho_{AH} = \alpha^{skew}\rho_{xx} + \sigma^{int}\rho_{xx}^2$, where α^{skew} and σ^{int} correspond to skew scattering parameter and intrinsic AHC respectively. σ^{int} was estimated $\sim$ 155 S/cm, which is about 70% of total AHC at 2 K. Thus, in the present system intrinsic Berry phase-driven K-L contribution dominates along with finite skew scattering [43–45].

4.3.4 Theoretical calculations

After obtaining the experimental value of AHC, we have theoretically calculated AHC for Co_2FeAl by setting the magnetization direction along [001]. For full Heusler alloys, the ground state energy in other magnetization directions like [110] was found close to the [001] direction and the band structure was also found quite similar in both directions, therefore the average picture of AHC is expected close to [001] direction [7, 9, 46, 47]. The intrinsic AHC is proportional to the Brillouin zone (BZ) summation of the Berry curvature over all occupied states [48].

$$\sigma^{\alpha\beta} = \frac{e^2}{\hbar}\frac{1}{N}\sum_{\boldsymbol{k}\in(BZ)} \Omega_\gamma(\boldsymbol{k}) f(\boldsymbol{k}), \tag{4.1}$$

where the indices α, β, and γ are the Cartesian coordinates. $f(\boldsymbol{k})$ stands for the Fermi distribution function, $\Omega_\gamma(\boldsymbol{k})$ denotes the γ component of the Berry curvature for the wave vector $\boldsymbol{k}$ and N is the number of electrons in the crystal. Further, the Berry curvature is related to the Berry connection $[A_n(\boldsymbol{k})]$ as

$$\Omega_n(\boldsymbol{k}) = \nabla_{\boldsymbol{k}} \times A_n(\boldsymbol{k}), \tag{4.2}$$

where "n" is the band index and $A_n(\boldsymbol{k})$ in terms of cell-periodic Bloch states $|u_{n\boldsymbol{k}}\rangle = e^{-ik.r}|\psi_{n\boldsymbol{k}}\rangle$ is defined as $A_n(\boldsymbol{k})$= $\langle u_{n\boldsymbol{k}}| \, i\boldsymbol{\nabla}_k \, |u_{n\boldsymbol{k}}\rangle$ [49]. In the first step of the AHC calculation, we considered the ordered $L2_1$ structure of Co_2FeAl i.e. without any disorder. As discussed earlier the intrinsic AHC of a system is strongly connected to its electronic band structure. In Fig. 4.5 (Top), we have compared the full electronic band structure of $L2_1$ ordered Co_2FeAl with the Wannier interpolated one. The better interpolation suggests that it will provide Wannier90-related properties accurately. The Wannier interpolation is a potential tool to calculate the momentum space integrals of rapidly varying functions [50]. Such integrals are involved in calculating properties such as anomalous Hall conductivity, spin Hall conductivity, orbital magnetization, and optical properties [51]. The most popular technique to construct the Wannier functions is the maximally localized method [52] which is implemented in the Wannier90 code [51]. The Wannier functions are generated using the unitary transformation of the Bloch wave function, so there is no loss of information during the generation. The main advantage of Wannier interpolation over other approaches is that it allows for the most

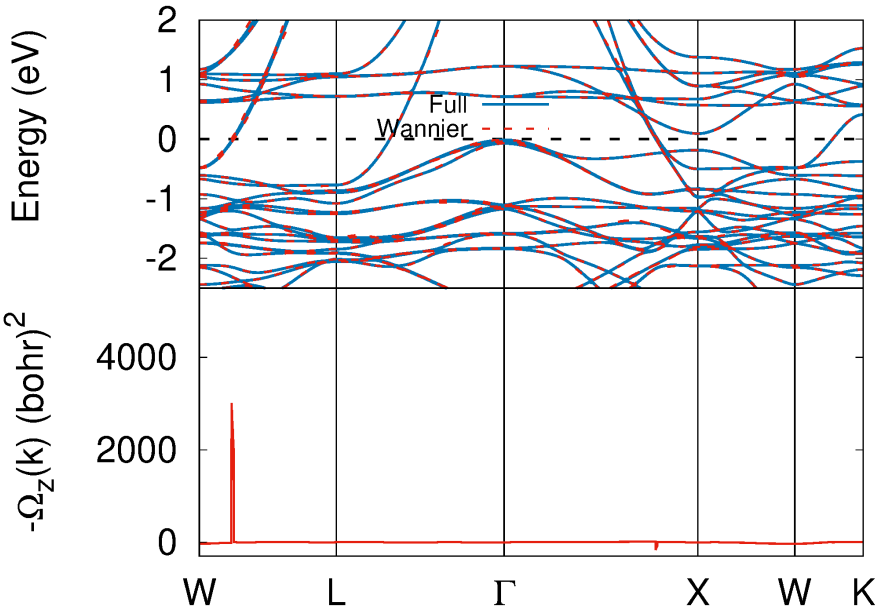

Figure 4.5: Top: Comparison of Wannier interpolated band structure (red) with the full electronic band structure (blue) of Co_2FeAl. The Fermi energy is set to 0 eV. Bottom: Calculated Berry curvatures along the high-symmetry path.

precise interpolation of band energies and matrix elements compared to other methods such as the tight-binding approach because there is no limitation in terms of the size of the basis set [53].

By this method, we found the theoretical value of AHC (σ^{xy}) about $\sim$ 42 S/cm, which is in good agreement with literature [54]. Thus the theoretical AHC considering ordered $L2_1$ structure is an order smaller than the experimental intrinsic AHC. Therefore, in the next step, we incorporated 50 % anti-site disorder between the Al and Fe sites (as observed from SXRD analysis) to compute AHC for the disordered Co_2FeAl. In Fig. 4.6 (Top), we have plotted the full electronic band structure of disordered Co_2FeAl with the Wannier interpolated band structure. The Berry curvature along the high symmetry path of disordered structure (space group $Pm\bar{3}m$) is depicted in Fig. 4.6 (Bottom). The intrinsic AHC (σ^{xy}) for disordered Co_2FeAl calculated from the integration of Berry curvature turned out to be $\sim$ 63 S/cm, which is interestingly larger than the ordered $L2_1$ structure. Thus, our theoretical calculations suggest that the disorder can modify the Berry curvature and result in an increased value of intrinsic AHC. Recently, it has been suggested in the literature that the presence of B2 disorder lowers the value of AHC in comparison to ordered $L2_1$ structure [12, 14]. Therefore, our combined experimental and theoretical results suggest that there is no straightforward rule that connects the Berry curvature to the disorder, rather it depends on the disorder-induced

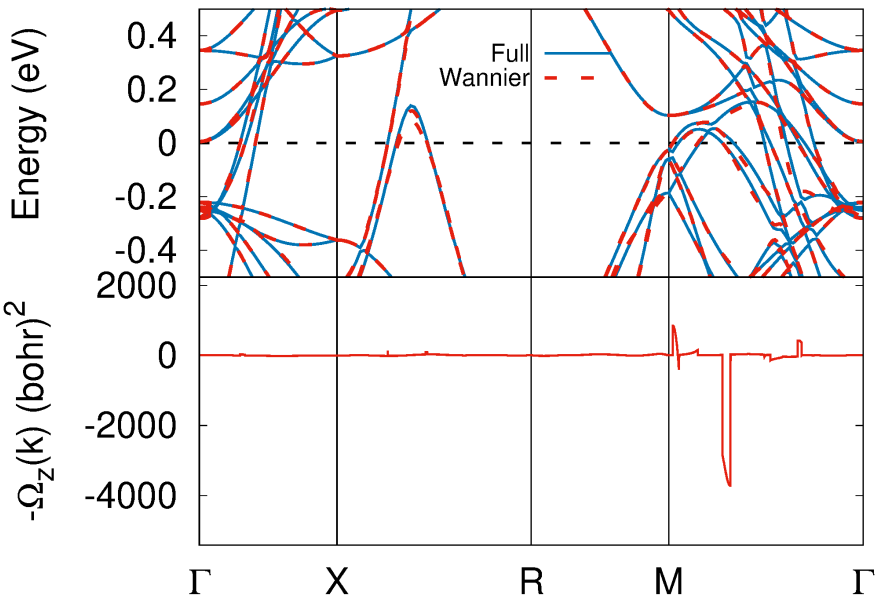

Figure 4.6: Top: Comparison of Wannier interpolated band structure (red) with the full electronic band structure (blue) of disordered Co_2FeAl. The Fermi energy is set to 0 eV. Bottom: Calculated Berry curvatures along the high-symmetry path.

change in electronic structure, which is different for different Heusler compounds as they have different numbers of electrons. If the effect of disorder is in such a way that it brings the band crossings or avoided band crossing very close to the Fermi energy then the value of Berry curvature will be large. We would also like to mention here that the experimentally found intrinsic AHC (155 S/cm) is larger than the theoretically predicted intrinsic AHC similar to the other metallic compounds [9, 43, 54, 55]. Hence, our results provide a platform for the systematic investigation of AHE in disordered Heusler compounds and related materials.

4.4 Conclusion

We investigated the anomalous transport properties of polycrystalline Co_2FeAl Heusler compound by experiment and theoretical calculations. SXRD data reveals a large degree of Fe-Al antisite disorder. Experimental values of AHC were found to be 227 S/cm at 2 K and 219 S/cm at 300 K with an intrinsic AHC of 155 S/cm. Our experimental analysis show that the AHE in Co_2FeAl is dominated by the intrinsic Berry phase mechanism. Our theoretical calculations suggest that the enhanced Berry curvature-induced intrinsic AHC is linked with the antisite disorder in Co_2FeAl Heusler compound.

References

[1] P. Brown, K.-U. Neumann, P. Webster, and K. Ziebeck, The magnetization distributions in some Heusler alloys proposed as half-metallic ferromagnets, J. Phys.: Condens. Matter **12**, 1827 (2000).

[2] I. Galanakis, P. Dederichs, and N. Papanikolaou, Slater-pauling behavior and origin of the half-metallicity of the full-Heusler alloys, Phys. Rev. B **66**, 174429 (2002).

[3] J. Kübler, G. Fecher, and C. Felser, Understanding the trend in the Curie temperatures of Co_2-based Heusler compounds: Ab initio calculations, Phys. Rev. B **76**, 024414 (2007).

[4] H. C. Kandpal, G. H. Fecher, and C. Felser, Calculated electronic and magnetic properties of the half-metallic, transition metal based Heusler compounds, J. Phys. D: Appl. Phys. **40**, 1507 (2007).

[5] S. Roy, R. Singha, A. Ghosh, A. Pariari, and P. Mandal, Anomalous Hall effect in the half-metallic Heusler compound Co_2TiX (X= Si, Ge), Phys. Rev. B **102**, 085147 (2020).

[6] H. Reichlova, R. Schlitz, S. Beckert, P. Swekis, A. Markou, Y.-C. Chen, D. Kriegner, S. Fabretti, G. Hyeon Park, A. Niemann, S. Sudheendra, A. Thomas, K. Nielsch, C. Felser, and S. T. B. Goennenwein, Large anomalous Nernst effect in thin films of the Weyl semimetal Co_2MnGa, Appl. Phys. Lett. **113**, 212405 (2018).

[7] P. Li, J. Koo, W. Ning, J. Li, L. Miao, L. Min, Y. Zhu, Y. Wang, N. Alem, C.-X. Liu, Z. Mao, and B. Yan, Giant room temperature anomalous Hall effect and tunable topology in a ferromagnetic topological semimetal Co_2MnAl, Nat. Commun. **11**, 3476 (2020).

[8] S. N. Guin, K. Manna, J. Noky, S. J. Watzman, C. Fu, N. Kumar, W. Schnelle, C. Shekhar, Y. Sun, J. Gooth, and C. Felser, Anomalous Nernst effect beyond the magnetization scaling relation in the ferromagnetic Heusler compound Co_2MnGa, NPG Asia Mater. **11**, 16 (2019).

[9] B. Ernst, R. Sahoo, Y. Sun, J. Nayak, L. Müchler, A. K. Nayak, N. Kumar, J. Gayles, A. Markou, G. H. Fecher, and C. Felser, Anomalous Hall effect and the role of Berry curvature in Co_2TiSn Heusler films, Phys. Rev. B **100**, 054445 (2019).

[10] J. Shen, Q. Yao, Q. Zeng, H. Sun, X. Xi, G. Wu, W. Wang, B. Shen, Q. Liu, and E. Liu, Local disorder-induced elevation of intrinsic anomalous Hall conductance in an electron-doped magnetic Weyl semimetal, Phys. Rev. Lett. **125**, 086602 (2020).

[11] E. V. Vidal, H. Schneider, and G. Jakob, Influence of disorder on anomalous Hall effect for Heusler compounds, Phys. Rev. B **83**, 174410 (2011).

[12] Y. Sakuraba, K. Hyodo, A. Sakuma, and S. Mitani, Giant anomalous Nernst effect in the $Co_2MnAl_{1-x}Si_x$ Heusler alloy induced by Fermi level tuning and atomic ordering, Phys. Rev. B **101**, 134407 (2020).

[13] J. Kudrnovskỳ, V. Drchal, and I. Turek, Anomalous Hall effect in stoichiometric Heusler alloys with native disorder: A first-principles study, Phys. Rev. B **88**, 014422 (2013).

[14] F. Mende, J. Noky, S. N. Guin, G. H. Fecher, K. Manna, P. Adler, W. Schnelle, Y. Sun, C. Fu, and C. Felser, Large anomalous Hall and Nernst effects in high curie-temperature iron-based Heusler compounds, Adv. Sci. **8**, 2100782 (2021).

[15] S. Husain, N. Sisodia, A. K. Chaurasiya, A. Kumar, J. P. Singh, B. S. Yadav, S. Akansel, K. H. Chae, A. Barman, P. Muduli, P. Svedlindh, and S. Chaudhary, Observation of skyrmions at room temperature in Co_2FeAl Heusler alloy ultrathin film heterostructures, Sci. Rep. **9**, 1085 (2019).

[16] X. Zhang, H. Xu, B. Lai, Q. Lu, X. Lu, Y. Chen, W. Niu, C. Gu, W. Liu, X. Wang, C. Liu, Y. Nie, L. He, and Y. Hu, Direct observation of high spin polarization in Co_2FeAl thin films, Sci. Rep. **8**, 8074 (2018).

[17] S. Husain, S. Akansel, A. Kumar, P. Svedlindh, and S. Chaudhary, Growth of Co_2FeAl Heusler alloy thin films on Si (100) having very small gilbert damping by ion beam sputtering, Sci. Rep. **6**, 28692 (2016).

[18] R. Malik, E. Delczeg-Czirjak, R. Knut, D. Thonig, I. Vaskivskyi, D. Phuyal, R. Gupta, S. Jana, R. Stefanuik, Y. Kvashnin,S. Husain,A. Kumar,Y. Svedlindh,J. Söderström,O. Eriksson, and O. Karis, Ultrafast magnetization dynamics in the half-metallic Heusler alloy Co_2FeAl, Phys. Rev. B **104**, L100408 (2021).

[19] A. Kumar, F. Pan, S. Husain, S. Akansel, R. Brucas, L. Bergqvist, S. Chaudhary, and P. Svedlindh, Temperature-dependent gilbert damping of Co_2FeAl thin films with different degree of atomic order, Phys. Rev. B **96**, 224425 (2017).

[20] S. Husain, A. Kumar, S. Akansel, P. Svedlindh, and S. Chaudhary, Anomalous Hall effect in ion-beam sputtered Co_2FeAl full Heusler alloy thin films, J. Magn. Magn. Mater. **442**, 288 (2017).

[21] X. Wang, Y. Li, Y. Du, X. Dai, G. Liu, E. Liu, Z. Liu, W. Wang, and G. Wu, Structural, magnetic and transport properties of Co_2FeAl Heusler films with varying thickness, J. Magn. Magn. Mater. **362**, 52 (2014).

[22] M. Kogachi, N. Tadachi, and T. Nakanishi, Structural properties and magnetic behavior in $CoFe_{1-x}Al_x$ alloys, Intermetallics **14**, 742 (2006).

[23] I.-M. Imort, P. Thomas, G. Reiss, and A. Thomas, Anomalous Hall effect in the Co-based Heusler compounds Co_2FeSi and Co_2FeAl, J. Appl. Phys **111**, 07D313 (2012).

[24] P. Giannozzi, S. Baroni, N. Bonini, M. Calandra, R. Car, C. Cavazzoni, D. Ceresoli, G. L. Chiarotti, M. Cococcioni, I. Dabo, A. D. Corso, S. de Gironcoli, S. Fabris, G. Fratesi, R. Gebauer, U. Gerstmann, C. Gougoussis, A. Kokalj, M. Lazzeri, L. Martin-Samos, N. Marzari, F. Mauri, R. Mazzarello, S. Paolini, A. Pasquarello, L. Paulatto, C. Sbraccia, S. Scandolo, G. Sclauzero, A. P. Seitsonen, A. Smogunov, P. Umari, and R. M. Wentzcovitch, QUANTUM ESPRESSO: a modular and open-source software project for quantum simulations of materials, J. Phys. Condens. Matter **21**, 395502 (2009).

[25] J. P. Perdew, K. Burke, and M. Ernzerhof, Generalized gradient approximation made simple, Phys. Rev. Lett. **77**, 3865 (1996).

[26] D. Hamann, Optimized norm-conserving vanderbilt pseudopotentials, Phys. Rev. B **88**, 085117 (2013).

[27] N. Marzari and D. Vanderbilt, Maximally localized generalized Wannier functions for composite energy bands, Phys. Rev. B **56**, 12847 (1997).

[28] I. Souza, N. Marzari, and D. Vanderbilt, Maximally localized Wannier functions for entangled energy bands, Phys. Rev. B **65**, 035109 (2001).

[29] R. Gupta, S. Husain, A. Kumar, R. Brucas, A. Rydberg, and P. Svedlindh, Co_2FeAl full Heusler compound based spintronic terahertz emitter, Adv. Opt. Mater. **9**, 2001987 (2021).

[30] B. K. Hazra, M. M. Raja, R. Rawat, A. Lakhani, S. Kaul, and S. Srinath, Effect of disorder on the anomalous Hall conductivity of Co_2Fesi thin films, J. Magn. Magn. Mater. **448**, 371 (2018).

[31] W. Kraus and G. Nolze, PowderCell-a program for the representation and manipulation of crystal structures and calculation of the resulting x-ray powder patterns, J. Appl. Crystallogr. **29**, 301 (1996).

[32] G. Ortiz, M. Gabor, T. Petrisor, Jr, F. Boust, F. Issac, C. Tiusan, M. Hehn, and J. Bobo, Static and dynamic magnetic properties of epitaxial Co_2FeAl Heusler alloy thin films, J. Appl. Phys. **109**, 07D324 (2011).

[33] S. Wurmehl, G. H. Fecher, K. Kroth, F. Kronast, H. A. Dürr, Y. Takeda, Y. Saitoh, K. Kobayashi, H.-J. Lin, G. Schönhense, and C. Felser, Electronic structure and spectroscopy of the quaternary Heusler alloy $Co_2Cr_{1-x}Fe_xAl$, J. Phys. D: Appl. Phys. **39**, 803 (2006).

[34] V. Jain, V. Jain, V. Sudheesh, N. Lakshmi, and K. Venugopalan, Electronic structure and magnetic properties of disordered Co_2FeAl Heusler alloy, in *AIP Conf Proc.* 1544-1545 (2014).

[35] X. Zhang, W. Liu, Y. Yan, W. Niu, B. Lai, Y. Zhao, W. Wang, L. He, H. Meng, and Y. Xu, The atomic-scale magnetism of Co_2FeAl Heusler alloy epitaxial thin films, Appl. Phys. Lett. **113**, 212401 (2018).

[36] A. Ahmad, S. Mitra, S. Srivastava, and A. Das, Size-dependent structural and magnetic properties of disordered Co_2FeAl Heusler alloy nanoparticles, J. Magn. Magn. Mater. **474**, 599 (2019).

[37] B. Fadila, M. Ameri, D. Bensaid, M. Noureddine, I. Ameri, S. Mesbah, and Y. Al-Douri, Structural, magnetic, electronic and mechanical properties of full-Heusler alloys Co_2YAl (Y=

Fe, Ti): first principles calculations with different exchange-correlation potentials, J. Magn. Magn. Mater. **448**, 208 (2018).

[38] A. Hirohata, M. Kikuchi, N. Tezuka, K. Inomata, J. Claydon, Y. Xu, and G. Van der Laan, Heusler alloy/semiconductor hybrid structures, Curr. Opin. Solid State Mater. Sci. **10**, 93 (2006).

[39] A. Markou, D. Kriegner, J. Gayles, L. Zhang, Y.-C. Chen, B. Ernst, Y.-H. Lai, W. Schnelle, Y.-H. Chu, Y. Sun, and C. Felser, Thickness dependence of the anomalous Hall effect in thin films of the topological semimetal Co_2MnGa, Phys. Rev. B **100**, 054422 (2019).

[40] P. Nozieres and C. Lewiner, A simple theory of the anomalous Hall effect in semiconductors, Journal de Physique **34**, 901 (1973).

[41] S. Onoda, N. Sugimoto, and N. Nagaosa, Intrinsic versus extrinsic anomalous Hall effect in ferromagnets, Phys. Rev. Lett. **97**, 126602 (2006).

[42] K. Manna, L. Muechler, T.-H. Kao, R. Stinshoff, Y. Zhang, J. Gooth, N. Kumar, G. Kreiner, K. Koepernik, R. Car, J. Kübler, G. H. Fecher, C. Shekhar, Y. Sun, and C. Felser, From colossal to zero: controlling the anomalous Hall effect in magnetic Heusler compounds via Berry curvature design, Phys. Rev. X **8**, 041045 (2018).

[43] Q. Wang, Y. Xu, R. Lou, Z. Liu, M. Li, Y. Huang, D. Shen, H. Weng, S. Wang, and H. Lei, Large intrinsic anomalous Hall effect in half-metallic ferromagnet $Co_3Sn_2S_2$ with magnetic Weyl fermions, Nat. Commun. **9**, 3681 (2018).

[44] D. Liu, A. Liang, E. Liu, Q. Xu, Y. Li, C. Chen, D. Pei, W. Shi, S. Mo, P. Dudin, P. Dudin, T. Kim, C. Cacho, G. Li, Y. Sun, L. X. Yang, Z. K. Liu, S. S. P. Parkin, C. Felser, and Y.L. Chen, Magnetic Weyl semimetal phase in a kagomé crystal, Science **365**, 1282 (2019).

[45] X. Chen, M. Wang, C. Gu, S. Wang, Y. Zhou, C. An, Y. Zhou, B. Zhang, C. Chen, Y. Yuan, M. Qi, L. Zhang, H. Zhou, J. Zhou, Y. Yao, and Z. Yang, Pressure-tunable large anomalous Hall effect of the ferromagnetic kagome-lattice Weyl semimetal $Co_3Sn_2S_2$, Phys. Rev. B **100**, 165145 (2019).

[46] P. Chaudhary, K. K. Dubey, G. K. Shukla, S. Singh, S. Sadhukhan, S. Kanungo, A. K. Jena,

S.-C. Lee, S. Bhattacharjee, J. Minár, and S. W. D'Souza, Role of chemical disorder in tuning the Weyl points in vanadium doped Co_2TiSn, Phys. Rev. Mater. **5**, 124201 (2021).

[47] Z. Wang, M. G. Vergniory, S. Kushwaha, M. Hirschberger, E. V. Chulkov, A. Ernst, N. P. Ong, R. J. Cava, and B. A. Bernevig, Time-reversal-breaking Weyl fermions in magnetic Heusler alloys, Phys. Rev. Lett. **117**, 236401 (2016).

[48] J. Kübler and C. Felser, Berry curvature and the anomalous Hall effect in Heusler compounds, Physical Review B **85**, 012405 (2012).

[49] G. Pizzi, V. Vitale, R. Arita, S. Blügel, F. Freimuth, G. Géranton, M. Gibertini, D. Gresch, C. Johnson, T. Koretsune, J. Ibañez-Azpiroz, H. Lee, J.-M. Lihm, D. Marchand, A. Marrazzo, Y. Mokrousov, J. I. Mustafa, Y. Nohara, Y. Nomura, L. Paulatto, S. Poncé, T. Ponweiser, J. Qiao, F. Thöle, S. S. Tsirkin, M. Wierzbowska, N. Marzari, D. Vanderbilt, I. Souza, A. A. Mostofi, and J. R. Yates, Wannier90 as a community code: new features and applications, J. Phys. Condens. Matter **32**, 165902 (2020).

[50] S. S. Tsirkin, High performance Wannier interpolation of Berry curvature and related quantities with WannierBerri code, npj Comput. Mater. **7**, 33 (2021).

[51] A. A. Mostofi, J. R. Yates, Y.-S. Lee, I. Souza, D. Vanderbilt, and N. Marzari, Wannier90: A tool for obtaining maximally-localised Wannier functions, Comput. Phys. Commun. **178**, 685 (2008).

[52] N. Marzari and D. Vanderbilt, Maximally localized generalized Wannier functions for composite energy bands, Phys. Rev. B **56**, 12847 (1997).

[53] S. Kundu, S. Bhattacharjee, S.-C. Lee, and M. Jain, Population analysis with Wannier orbitals, J. Chem. Phys. **154**, 104111 (2021).

[54] H.-L. Huang, J.-C. Tung, and G.-Y. Guo, Anomalous Hall effect and current spin polarization in Co_2FeX Heusler compounds (X= Al, Ga, In, Si, Ge, and Sn): A systematic ab initio study, Phys. Rev. B **91**, 134409 (2015).

[55] Y. Zhu, B. Singh, Y. Wang, C.-Y. Huang, W.-C. Chiu, B. Wang, D. Graf, Y. Zhang, H. Lin, J. Sun, A. Bansil, and Z. Mao, Exceptionally large anomalous Hall effect due to anticrossing

of spin-split bands in the antiferromagnetic half-Heusler compound TbPtBi, Phys. Rev. B **101**, 161105 (2020).